

# **NIST Technical Note XXXX**

## **Mapping the Chemical Structure of Centerline Profiles in Medium-Scale Pool Fires**

Ryan Falkesntein-Smith  
Anthony Hamins  
Kunhyuk Sung  
Jian Chen

This publication is available free of charge from:  
<https://doi.org/10.6028/NIST.TN.XXXX>



# NIST Technical Note XXXX

## Mapping the Chemical Structure of Centerline Profiles in Medium-Scale Pool Fires

Ryan Falkenstein-Smith

Anthony Hamins

Kunhyuk Sung

Jian Chen

*Fire Research Division  
Engineering Laboratory*

This publication is available free of charge from:  
<https://doi.org/10.6028/NIST.TN.XXXX>

August 2019



U.S. Department of Commerce  
Wilbur L. Ross, Jr., Secretary

National Institute of Standards and Technology

Walter Copan, NIST Director and Undersecretary of Commerce for Standards and Technology

Certain commercial entities, equipment, or materials may be identified in this document in order to describe an experimental procedure or concept adequately. Such identification is not intended to imply recommendation or endorsement by the National Institute of Standards and Technology, nor is it intended to imply that the entities, materials, or equipment are necessarily the best available for the purpose.

**National Institute of Standards and Technology Technical Note XXXX**  
**Natl. Inst. Stand. Technol. Tech. Note XXXX, 29 pages (August 2019)**  
**CODEN: NTNOEF**

**This publication is available free of charge from:**  
**<https://doi.org/10.6028/NIST.TN.XXXX>**

## **Abstract**

This report documents a series of time-averaged local gas species measurements made throughout the centerline profile of moderate-sized methanol, ethanol, and acetone pool fires steadily burning in a quiescent environment. All gas species measurements are obtained using a Gas Chromatograph/ Mass Spectrometer system (GC/MSD). The volume fraction of each species was calculated via the number of moles identified by the GC/MSD at each location throughout the centerline profile of the fire. Soot mass fractions are measured during the gas sampling process. The gas species volume and soot mass fractions were compared at different heights within the fire and across a variety of different fuels.

## **Key words**

Acetone fuel, Ethanol fuel, Gas species measurements. Methanol fuel, Moderate-sized pool fire

# Table of Contents

<b>1</b>	<b>Introduction</b>	<b>4</b>
<b>2</b>	<b>Description of Experiments</b>	<b>4</b>
2.1	Pool Burner Setup	5
2.2	Measuring the Volume Fraction of Gas Species via GC/MSD	6
2.3	Determining Soot Mass Fraction	9
<b>3</b>	<b>Mixture Fraction</b>	<b>11</b>
<b>4</b>	<b>Results</b>	<b>12</b>
4.1	Flame Observations	12
4.2	Gas Species Concentrations	12
4.3	Soot Mass Fraction	14
4.4	Mixture Fraction Results	14
4.5	Carbon Balance	14
<b>5</b>	<b>Conclusion</b>	<b>14</b>
<b>References</b>		<b>19</b>
<b>A</b>	<b>Uncertainty Analysis of Gas Species Concentrations</b>	<b>20</b>
<b>Appendix A: Uncertainty Analysis of Gas Species Concentrations</b>		<b>20</b>
A.1	Number of Moles of a Given Species	20
A.2	Total Number of Moles Identified	20
<b>B</b>	<b>Uncertainty Analysis of Gas Species Calibrations</b>	<b>21</b>
<b>Appendix B: Uncertainty Analysis of Gas Species Calibrations</b>		<b>21</b>
B.1	Total Moles Injected into the GC/MSD for Calibration	22
B.2	Table of Gas Standards with Error	23
B.3	Concentration of Vapors from Bubblers	24
<b>C</b>	<b>Uncertainty Analysis of the Soot Mass Fraction</b>	<b>26</b>
<b>Appendix C: Uncertainty Analysis of the Soot Mass Fraction</b>		<b>26</b>
C.1	Mass of Soot	26
C.2	Mass Flow Controller Volumetric Flow Rate	26
C.3	GC/MSD Sample Loop Volume	27
C.4	Total Mass Injected into the GC/MSD	27
C.5	Mass Flow Controller Internal Gas Flow Temperature Reading	27
C.6	Temperature Reading at the Entrance of the Probe	27
<b>D</b>	<b>Uncertainty Analysis of the Mixture Fraction</b>	<b>28</b>
<b>Appendix D: Uncertainty of the Mixture Fraction</b>		<b>28</b>
<b>E</b>	<b>Uncertainty Analysis of Pool Fire Parameters</b>	<b>29</b>
<b>Appendix E: Uncertainty of Pool Fire Parameters</b>		<b>29</b>
E.1	Mass Burning Flux	29

E.2	Heat Release Rate	29
E.3	Mean Flame Height	29

## List of Tables

Table 1	List of measurements obtained in a well-ventilated round, steady, 30.0 cm diameter pool fire burning in a quiescent environment. The uncertainty of measurements of fire parameters are discussed in detail in Appendix E.	14
Table 2	Gas Standards used to Calibrate GC/MSD	23
Table 3	Liquid Vapor Pressure Correlation Coefficients for Various Calibrated Liquids	25

## List of Figures

Fig. 1	Pool Burner Design	5
Fig. 2	Monitoring Fuel Level	7
Fig. 3	A schematic of the gas sampling procedure	8
Fig. 4	Process for cleaning soot probe	11
Fig. 5	Pool Fire Structures	13
Fig. 6	Major Species Comparison	15
Fig. 7	Averaged quasi-steady mass fraction of major species as a function of mixture fraction for a methanol pool fire	16
Fig. 8	Averaged quasi-steady mass fraction of major species as a function of mixture fraction for an ethanol pool fire	17
Fig. 9	Averaged quasi-steady mass fraction of major species as a function of mixture fraction for a acetone pool fire	18
Fig. 10	Flow diagram for bubble calibration system used for liquid materials	24

## 1. Introduction

Use of fire modeling, such as the Fire Dynamic Simulator (FDS) [1], in fire protection engineering, has increased dramatically during the last decade due to the development of practical computational fluid dynamics fire models and the decreased cost of computational power. Today, fire protection engineers use models to design safer buildings, nuclear power plants, aircraft cabins, trains, and marine vessels, to name a few types of applications. To be reliable, the models require validation, which involves an extensive collection of experimental measurements. An objective of this report is to provide data for use in fire model evaluation by the research community.

A pool fire is a fundamental combustion configuration of interest in model development. In pool fires, the fuel surface is isothermal, flat and horizontal, which provides a well-defined and straightforward setup for testing models and furthering the understanding of fire phenomena. In moderate and large-scale pool fires, radiative heat transfer is the dominant mechanism of heat feedback to the fuel surface. Species concentrations and temperatures have a significant influence on the radiative heat transfer. A zone of particular interest is the fuel rich-core between the flame and the pool surface, where gas species can absorb energy that would otherwise have been transferred to the fuel surface. Few studies in the literature studies have reported local chemical species measurements, which provide a deep understanding of the chemical structure of a pool fire and provide insight on critical kinetic, heat, and mass transfer processes.

The purpose of this study is to characterize the spatial distribution of stable gas-phase chemical species in a moderate-scale liquid pool fire steadily burning in a well-ventilated quiescent environment. Here, methanol, ethanol, and acetone are the fuels of interest. Contrary to ethanol and acetone, fires established using methanol are unusual as no carbonaceous soot is present or emitted.

In this study, measurements are made in a 30.0 cm diameter pool fire using various fuels. These particular fires are selected for research since the measurements complement results from previous studies, including analyses of the mass burning rate, the temperature and velocity fields, radiative emission, flame height, and pulsation frequency [2, 3]. Additional characterization of this fire enables a more comprehensive understanding of its detailed structure, enhancing the understanding of fire physics.

## 2. Description of Experiments

The methods used in this work to investigate pool fires have been documented previously [3–7]. Experiments are conducted under a canopy hood surrounded by a 2.5 m x 2.5 m x 2.5 m enclosure made of a double-mesh screen wall. The walls of the enclosure were formed by a double layer of the wire-mesh screen (5 mesh/cm) that reduced the influence of compromising room flows that could disrupt the pool fire's flow field. All measurements were made once the burning conditions, specifically the mass burning rate, reached steady-state, achieved approximately 10 min after ignition.

## 2.1 Pool Burner Setup

A circular, stainless-steel pan with an outer diameter of 30.0 cm, a depth of 15.0 cm, and a wall thickness of 0.16 cm was used as the pool burner. As shown in Fig. 1, the burner was placed within an overflow basin, which extended 3.00 cm beyond the burner wall. The burner is fitted with legs such that the burner rim was positioned 30 cm above the ground. The bottom of the burner was maintained at a constant temperature by flowing water ( $20^{\circ}\text{C} \pm 3^{\circ}\text{C}$ ) through a 3 cm section on the bottom of the fuel pan. Additionally, a fuel level indicator was positioned near the center of the burner to aid in maintaining the fuel level while burning.

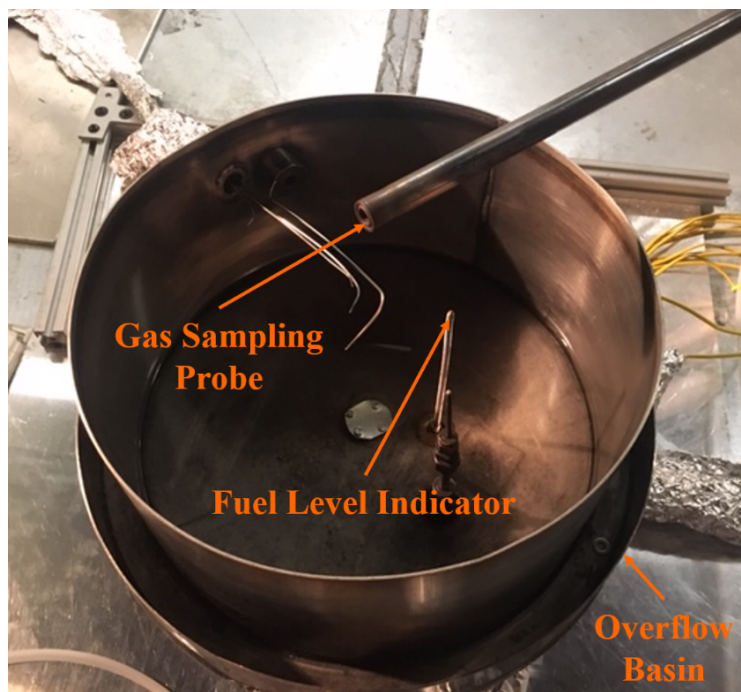


**Fig. 1.** A 30 cm Pool Burner with fuel level indicator, overflow section, and quenching probe

The time-averaged mass burning flux,  $m''$ , was determined from the rate at which fuel was delivered to the pool. Fuel to the burner was gravity fed from a reservoir positioned on a mass load cell located outside the enclosure and monitored by a data acquisition system. Figure 2 shows the procedure for monitoring the fuel level via fuel flow operator. Using a live video feed, the operator was able to observe a close up of a slightly discernable dimple (Approximately 2 mm) made from the fuel level indicator on the fuel surface. The fuel level was controlled at 10 mm below the burner rim by manually adjusted the fuel flow using a needle valve.

The expanded uncertainty of the mass burning rate was estimated from a combination of Type A and B evaluation of standard uncertainty. The Type A evaluation of standard uncertainty was determined from the variance in the time-averaged mass burning flux mea-

sured during each test. The Type B evaluation of standard uncertainty was defined as the bias errors in the load cell used to measure the mass flux. The uncertainty of the mass burning flux is discussed further detail in Appendix E.1.

The heat release rate of each fuel,  $\dot{Q}$ , was calculated from Eq.1 using the time-averaged mass burning flux measurements:

$$\dot{Q} = m'' \Delta H_c A \quad (1)$$

where  $\Delta H_c$  is the heat of the combustion of the burned fuel provided by DIPPR® and  $A$  is the cross-sectional area of the pool fire. The uncertainty of the heat release rate was calculated from the law of propagation of uncertainty which is detailed in Appendix E.2.

The mean flame height was estimated from 3600 frames obtained from high quality video recordings of the methanol, ethanol, and acetone pool fire tests. Frames were processed using MATLAB's Image Processing Toolbox. Imported RGB images were decomposed into binary (black and white) images using a pre-set threshold level. The flame height for a single frame was defined as the distance between the pool surface and flame tip established using MATLAB software. The measurement was reapeated for each of the 3600 frames then averaged to provide the mean flame height.

The uncertainty of the mean flame height was estimated by combing the Type A and B evaluation of uncertainty defined as the variance of the averaged height measurements from each frame and the bias error of the distance measured in each frame. A detailed description of the uncertainty analysis for the mean flame height is described in Appendix E.3.

## 2.2 Measuring the Volume Fraction of Gas Species via GC/MSD

Gas-species measurements were made using an Agilent 5977E Series GC/MSD fitted with a thermal conductivity detector (TCD). The GC/MSD was able to quantify a variety of stable reactants, intermediates, and combustion product species collected from the pool fire. The GC/MSD was equipped with a 2 ml sample loop maintained at a 200 °C. Chromatographic separation of species was achieved using a Select for Permanent Gases-Dual Column (CP7430) comprised of mole-sieve and Porapak Q columns working in parallel and using a helium carrier gas. The sample analysis time was 62 min wherein the carrier gas flow leading into the TCD and MSD was 3.00 ml/min and 1.00 ml/min, respectively. During the analysis, the GC oven temperature was maintained at 30 °C for 12 min, then ramped at 8 °C/min for 2 min until a temperature of 300 °C was obtained.

Figure 3 displays the flow diagram for gas sampling into the GC/MSD. After achieving steady-state burning conditions, approx. 10 min after ignition, flow prompted by a vacuum pump located downstream from the GC/MSD was initiated. Gas samples were collected using a quenching probe. The quenching probe was composed of two concentric, stainless-steel tubes with outer annular coolant flow and inner, extracted, gas-sample flow. The inner and outer tube diameters were 7.9 mm and 16 mm, respectively. Water at 90 °C flowed through the sampling probe for the duration of the experiment. The remainder of



**Fig. 2.** Photo of fuel flow operators monitoring the fuel level via live video feed (top) and a close up image of the live video feed used to maintain a consistent fuel level relative to the fuel level indicator (bottom)

the sampling line leading into the GC/MSD was heated with electrical, heating tape to 140 °C to prevent condensation of water and liquid fuels through the line.

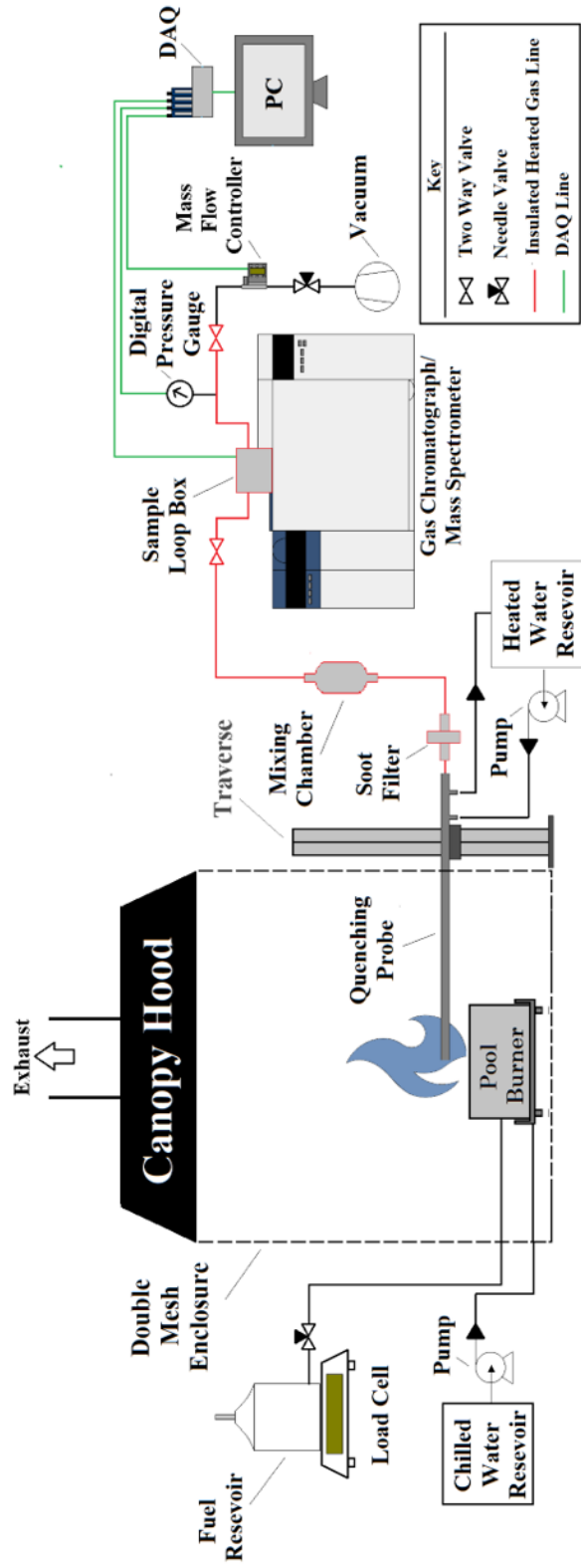


Fig. 3. A schematic of the extractive sampling setup used to transport gas samples from the pool fire to the GC/MSD

Gas sampling was conducted for a minimum of 12 min, ensuring that the gas sample had completely swept through the GC/MSD sample loop. The gas sampling period varied from 12 min to 25 min depending on the sampling location within the fire. The sampling flow was controlled using a mass flow controller (Alicat Scientific MC-Series) located in front of the vacuum pump within the sampling line. During the gas sampling procedure, the volumetric flow was approximately 200 ml/min and recorded using DAQ at 2 Hz for the entire duration of the gas sampling procedure. The mass flow controller also provided temperature readings of its internal gas flow.

After the gas sampling period, two quarter-turn valves located on opposite ends of the GC/MSD sample loop within the sampling line are closed. Once the sampled gas reached equilibrium, pressure measurements, obtained from a digital pressure gauge (OMEGA DPG409-030DWU), and temperature measurements, acquired by a K Type Thermocouple located at the GC/MSD Sample Loop injection port, were collected at 2 Hz for 50 s. After collecting pressure and temperature measurements, the sampled gas was injected into the GC/MSD.

The volume fraction,  $\bar{X}_i$ , was calculated from the ratio between the number of moles of a given gas species,  $n_i$ , and the total number of moles identified,  $n_{tot}$ . The moles of a given species were measured from the Thermal Conductivity Detector (TCD) within the GC/MSD. The total number of moles was determined from the summation of moles for each species identified by the TCD.

$$\bar{X}_i = \frac{n_i}{n_{tot}} \quad (2)$$

The mass fraction,  $\bar{Y}_i$ , of each species  $i$  was calculated from the measured volume fraction,  $\bar{X}_i$ , using the following expression:

$$\bar{Y}_i = \frac{\bar{X}_i \text{ } MW_i}{MW_{tot}} \quad (3)$$

where  $MW_i$  is the molecular weight of a given species and  $MW_{tot}$  is the average molecular weight of all detected gas species represented in the function below.

$$MW_{tot} = \sum \bar{X}_i \text{ } MW_i \quad (4)$$

All measurements using the GC/MSD were repeated at least twice at each location along the centerline of the pool fire. Gas species concentration measurements made at the same location were averaged. The variance in the gas species volume fraction was a function of location and species. A detailed description of the uncertainty analysis for the gas species measurement and its calibration is discussed in Appendices A and B, respectively.

### 2.3 Determining Soot Mass Fraction

Soot was collected simultaneously with gas samples using the sampling procedure described in Section 2.2. Before a test, a dessicated 47 mm Polytetrafluoroethylene (PTFE)

filter was weighed and subsequently placed into an in-line stainless steel particulate filter holder [8]. During a test, the filter holder was positioned within the gas sampling line behind the quenching probe and heated to 140 °C using heating tape to prevent condensation of water and liquid fuels on the filter. After testing, the PTFE filter was removed from the filter holder and dried in a desicator. After desiccating for 48 hrs, the PTFE filter's final weight was measured. Approximately 2 mg of soot was collected during the gas sampling period which varied from 12 min to 25 min depending on the sampling location within the fire.

After some tests, soot deposits were observed on the inner walls of the quenching probe. As shown in Fig. 4 desiccated gun cleaning patches were used to clean the inside of the quenching probe. At least two patches were used to collect soot on the inside of the probe. Soot collection using patches concluded once a patch was observed to have no soot after being swept through the inner walls of the quenching probe. Patches were weighed immediately before and 48 hrs after cleaning the inside of the probe. The soot collected from the dry patches was accounted for when calculating the soot mass fraction. The portion of the soot collected on the inner walls of the quenching probe relative to the PTFE filter varied based on the sampling location. The mass of the PTFE filter and cleaning patches were measured three times before and after each test.

The soot mass fraction,  $M_s$ , was computed from the mass of the soot collected from the PTFE filter and gun cleaning patches,  $m_s$ , the ratio of the mass flow controller's temperature reading,  $T_\infty$ , to the temperature at the probe entrance,  $T_p$ , the total mass of gas sampled,  $M_t$ , based on the mass flow controller readings:

$$M_s = \frac{m_s}{M_t} \frac{T_\infty}{T_p} \quad (5)$$

The total mass of gas sampled was estimated from product of the average volumetric flow rate measured by the mass flow controller,  $\dot{V}$ , the density of the sample gas injected into the GC/MSD,  $\rho_g$ , and the gas sampling time,  $t$ .

$$M_t = \dot{V} \cdot \rho_g \cdot t \quad (6)$$

In Eq.6, the density of the sample gas was determined from the total mass detected in the TCD chromatogram,  $m_{tot}$ , for the injected sample volume,  $V_s$ .

$$\rho_g = \frac{m_{tot}}{V_s} \quad (7)$$

The uncertainty of the soot mass fraction was estimated from a combined uncertainty of the Type A evaluation of standard uncertainty in the variation of temperature and mass measurements and the Type B standard uncertainty in the bias errors of the instrumentation. A detailed description of the soot mass fraction uncertainty is provided in Appendix C.



**Fig. 4.** Process of collecting soot from the internal walls of the quenching probe using gun cleaning patches

### 3. Mixture Fraction

The mixture fraction,  $Z$ , was based on carbon containing species and was defined as follows:

$$Z = Y_F + \frac{MW_F}{x} \sum \frac{Y_i}{MW_i} \quad (8)$$

where  $Y_F$ ,  $MW_F$ , and  $x$  are the mass fraction, molecular weight, and number of carbon molecules of the parent fuel, respectively. Considering the idealized reaction of a hydro-carbon fuel, the state reactions was derived as:

$$\begin{aligned} C_xH_yO_z + \eta \left( x + \frac{y}{4} - \frac{z}{2} \right) (O_2 + 3.76 N_2 + 0.0445 Ar) \\ \rightarrow max(0, 1 - \eta) C_xH_yO_z + max(0, 1 - \eta) \left( x + \frac{y}{4} - \frac{z}{2} \right) O_2 + min(1, \eta) x CO_2 \\ + min(1, \eta) \frac{y}{2} H_2O + \eta \left( x + \frac{y}{4} - \frac{z}{2} \right) (3.76 N_2 + 0.0445 Ar) \end{aligned} \quad (9)$$

where  $\max(\alpha, \beta)$  and  $\min(\alpha, \beta)$  are operators that return the larger and smaller value, respectively, of the two parameters  $\alpha$  and  $\beta$ . The parameter  $\eta$  represents the portion of air relative to the amount of fuel used as a reactant in Eq. 9. In other words,  $\eta$  can be defined as the reciprocal of the local fuel equivalence ratio,  $\phi$ ,

$$\phi = \frac{(F/A)}{(F/A)_{st}} = \frac{1}{\eta} \quad (10)$$

where  $F/A$  is the fuel-air ratio and the subscript  $st$  denotes the stoichiometric condition. The idealized mixture fractions of the products relative to the mixture fraction can then be calculated through a combination of Eq. 8 and 9.

The uncertainty of the mixture fraction was determined from propagating the error in the mass fraction measurements. A detailed description of the mixture fraction uncertainty is provided in Appendix D.

## 4. Results

Brief observations of each pool fire burning different fuels are described in the first portion of this section. The key results of this work are the local gas species and soot measurements made at incremental heights along the centerline of medium-scale pool fires using various fuels such as methanol, ethanol, and acetone. A more in-depth analysis of the relationships between different measured gas is also provided in this section.

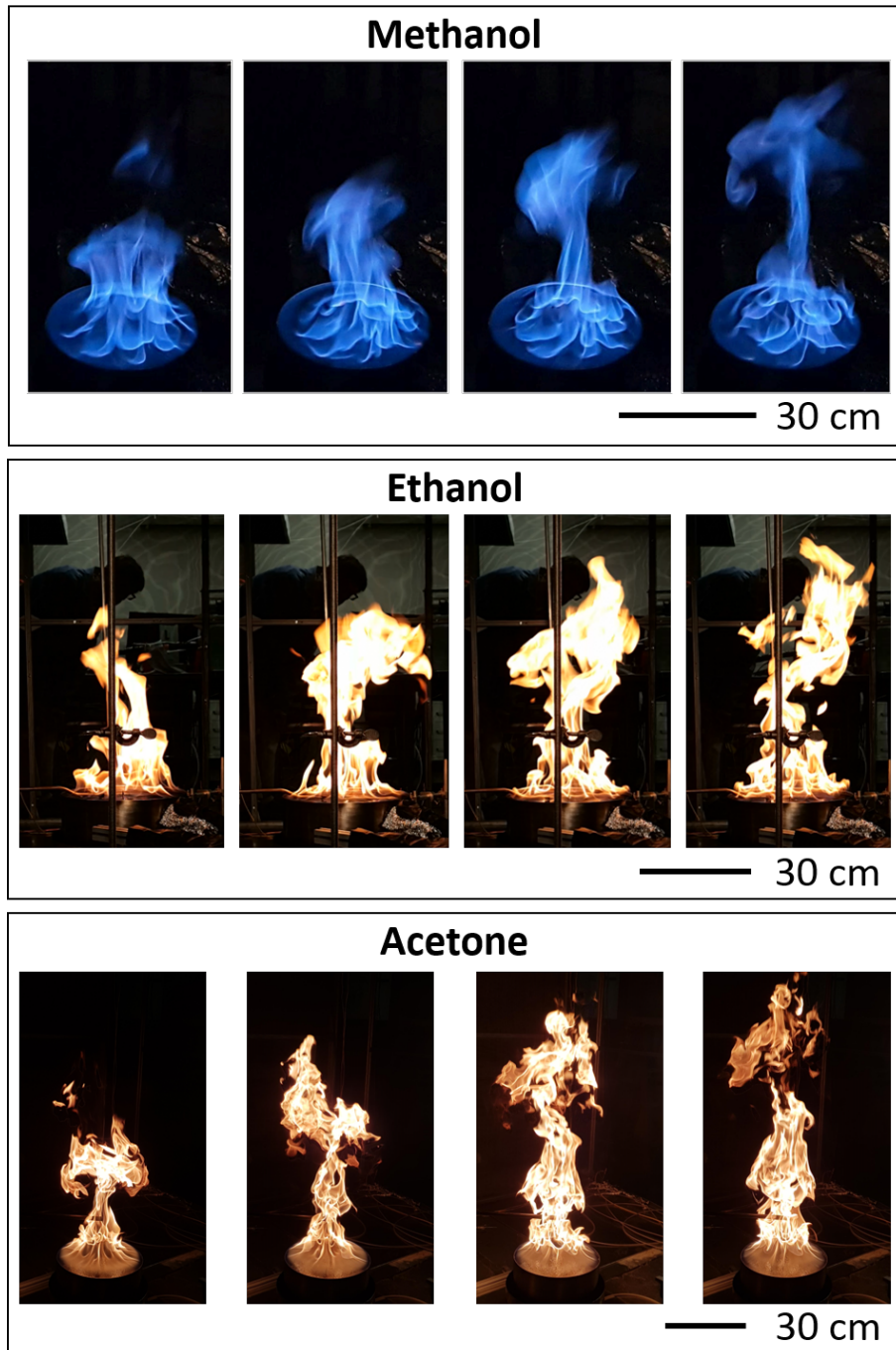
### 4.1 Flame Observations

Figure 5 displays a series of snapshots depicting the flame pulsation of the methanol, ethanol, and acetone pool fires in the 30.0 cm stainless-steel water-cooled burner. A repeated cycle was observed in each of the pool fires; uniformly curved flame sheets present at the burner rim would roll towards the fire centerline to form a long and narrow plume.

The shape and visible color of the fires differed between fuel types. The methanol fire appeared to be completely blue, whereas the ethanol and acetone fires primarily consisted of vibrant yellow and orange colors. The methanol pool fire was observed to exhibit a weak turbulent structure compared to the fully developed fires of the other two fuels. The observed dynamic shapes were consistent with previous experiments [3–7]. Table 1 provides a list of measurements made of each pool fire. The observed provide in the Table below are consistent with previous works [9].

### 4.2 Gas Species Concentrations

Figure 6 displays the averaged volume fraction,  $\bar{X}_i$ , of significant species measurements made at various heights along the methanol, ethanol, and acetone fire centerlines. Significant species detected in the TCD chromatogram include reactants, fuels and oxygen ( $O_2$ ),



**Fig. 5.** Flame structures of methanol (top), ethanol (middle), and acetone (bottom) pool fires during their pulsing cycles

**Table 1.** List of measurements obtained in a well-ventilated round, steady, 30.0 cm diameter pool fire burning in a quiescent environment. The uncertainty of measurements of fire parameters are discussed in detail in Appendix E.

Parameter (units)	Methanol	Ethanol	Acetone
Mass Burning Flux (g/m <sup>2</sup> s)	12.4 ± 1.1	13.9 ± 0.8	17.6 ± 2.7
Heat Release Rate (kW)	17.4 ± 1.4	26.3 ± 1.5	35.5 ± 5.4
Mean Flame Height (cm)	36.4 ± 16.0	61.1 ± 28.2	91.5 ± 34.6

combustion products such as water ( $H_2O$ ) and carbon dioxide ( $CO_2$ ), combustion intermediates such as carbon monoxide ( $CO$ ), hydrogen ( $H_2$ ), methane ( $CH_4$ ), and inert gases such as Nitrogen ( $N_2$ ) and Argon ( $Ar$ ).

As expected, the fuel volume fractions were highest, and the oxygen volume fraction was the lowest close to the fuel surface. The product species were found to have a maximum volume fraction at approximately 4 cm above the fuel surface. The intermediate gas species were found to have peaked at approximately 2 cm above the fuel surface. Inert gases were shown to increase with the distance from the fuel surface. It was also found that the gas sampled from the centerline nearly mimicked the composition of air at approximately 60 cm above the fuel surface.

#### 4.3 Soot Mass Fraction

#### 4.4 Mixture Fraction Results

#### 4.5 Carbon Balance

### 5. Conclusion

### Acknowledgments

The authors would like to acknowledge Kimberly Harris of the Gas Sensing Metrology Group at NIST, who assisted in the developing the species calibration method used in the study.

### Pool Fire Comparison, Centerline Product Species Concentrations

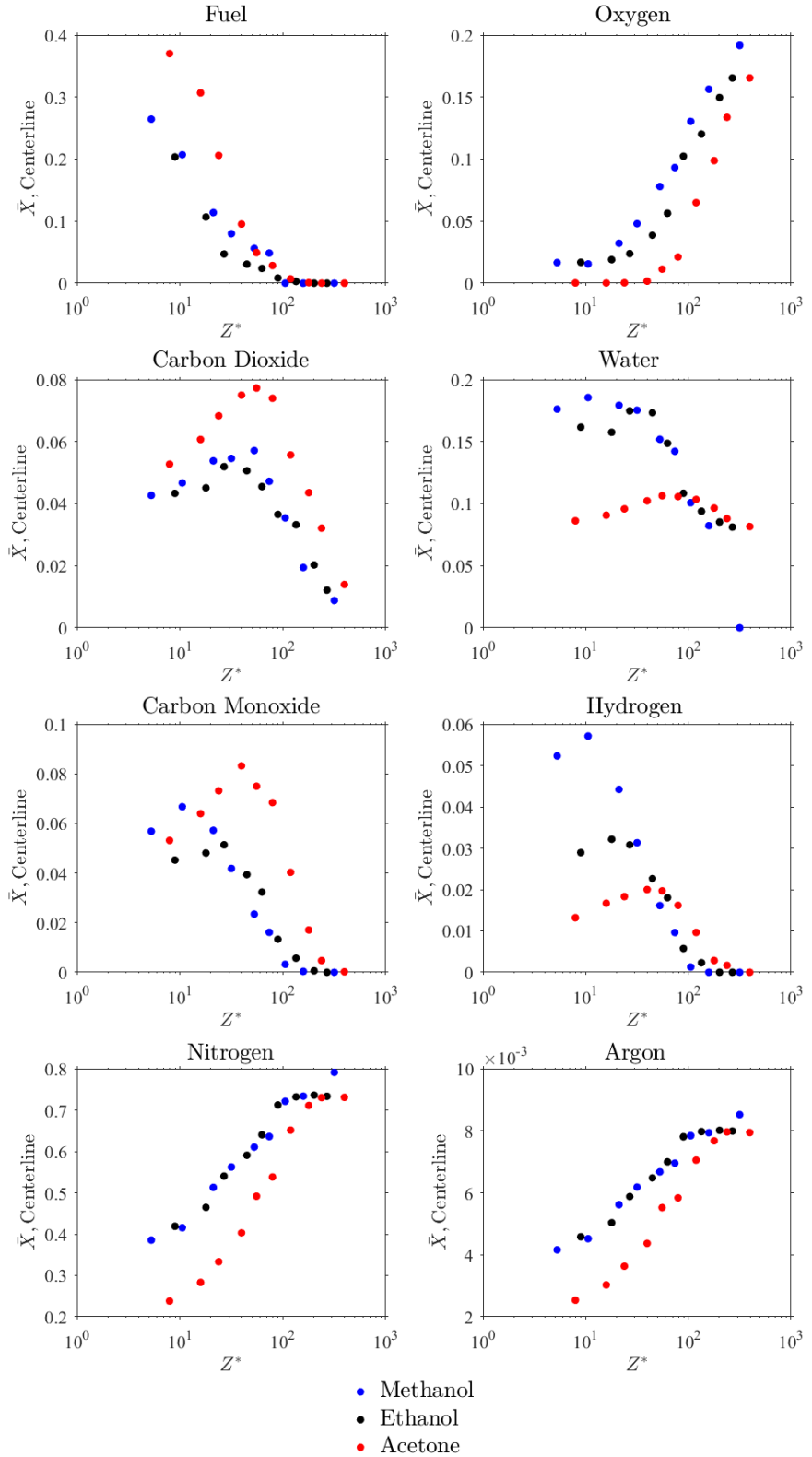


**Fig. 6.** Flame structures of methanol (top), ethanol (middle), and acetone (bottom) pool fires during their pulsing cycles

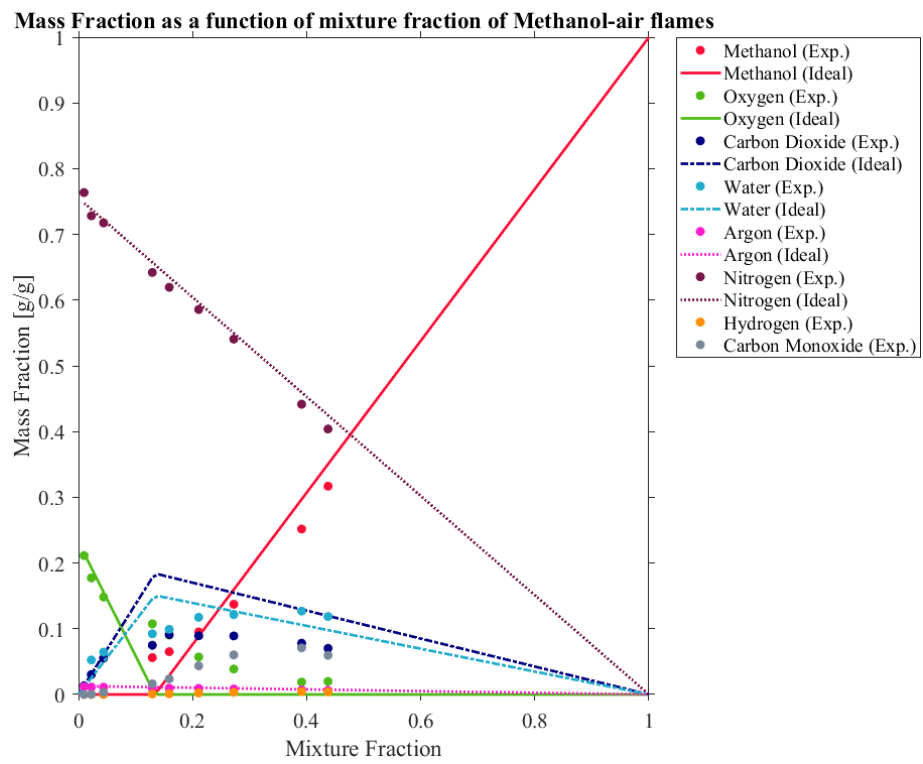


**Fig. 7.** Mass fractions of major species detected from a methanol pool fire centerline as a function of mixture fracton

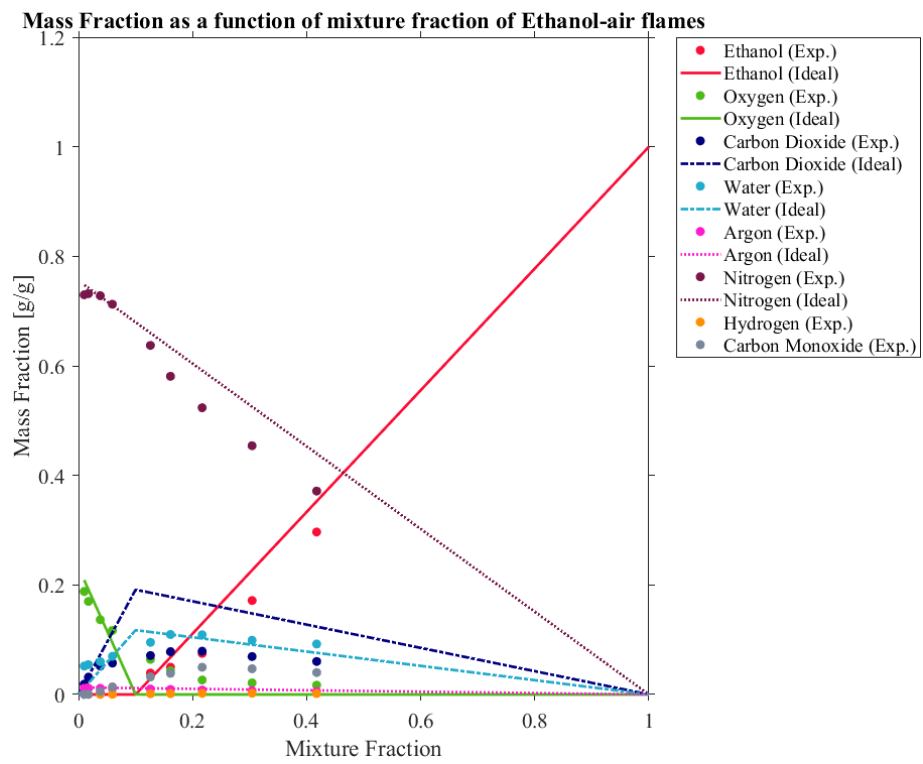


**Fig. 8.** Mass fractions of major species detected from a ethanol pool fire centerline as a function of mixture fracton

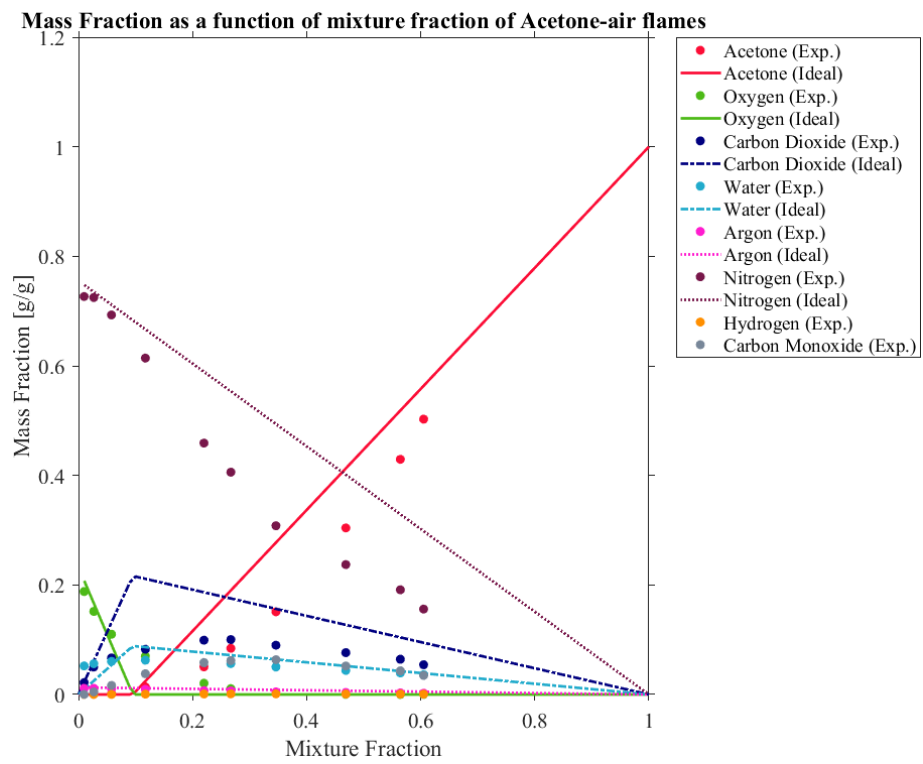


**Fig. 9.** Mass fractions of major species detected from a acetone pool fire centerline as a function of mixture fracton

## References

- [1] McGrattan K, Hostikka S, McDermott R, Floyd J, Weinschenk C, Overholt K (2013) *Fire Dynamics Simulator, Technical Reference Guide* National Institute of Standards and Technology, Gaithersburg, Maryland, USA, and VTT Technical Research Centre of Finland, Espoo, Finland, sixth Ed. Vol. 1: Mathematical Model; Vol. 2: Verification Guide; Vol. 3: Validation Guide; Vol. 4: Software Quality Assurance.
- [2] Fischer S, Hardouin-Duparc B, Grosshandler W (1987) The structure and radiation of an ethanol pool fire. *Combustion and Flame* 70(3):291–306. [https://doi.org/10.1016/0010-2180\(87\)90110-6](https://doi.org/10.1016/0010-2180(87)90110-6)
- [3] Hamins A, Lock A (2016) *The Structure of a Moderate-Scale Methanol Pool Fire* (US Department of Commerce, National Institute of Standards and Technology), .
- [4] Hamins A, Fischer S, Kashiwagi T, Klassen M, Gore J (1994) Heat feedback to the fuel surface in pool fires. *Combustion Science and Technology* 97(1-3):37–62.
- [5] Hamins A, Klassen M, Gore J, Kashiwagi T (1991) Estimate of flame radiance via a single location measurement in liquid pool fires. *Combustion and flame* 86(3):223–228.
- [6] Hamins A, Kashiwagi T, Buch R (1996) Characteristics of pool fire burning. *Fire resistance of industrial fluids* (ASTM International), , .
- [7] Lock A, Bundy M, Johnsson E, Hamins A, Ko G, Hwang C, Fuss P, Harris R (2008) Experimental study of the effects of fuel type, fuel distribution, and vent size on full-scale underventilated compartment fires in an iso 9705 room. *NIST TN* 1603.
- [8] Corporation P (2019) 47 mm In-line Filter Holder, Aluminum. Available at <https://shop.pall.com/us/en/laboratory/microbiological-qc/equipment-pumps-manifolds-spare-parts/47-mm-in-line-filter-holder-aluminum-zidgri78m8o>.
- [9] Kim SC, Lee KY, Hamins A (2019) Energy balance in medium-scale methanol, ethanol, and acetone pool fires. *Fire Safety Journal* .

## A. Uncertainty Analysis of Gas Species Concentrations

As shown in Eq. 2, volume fraction,  $\bar{X}_i$  was calculated from the ratio between the number of moles of a given species,  $n_i$ , and the total number of moles identified,  $n_{tot}$ . The uncertainty of the measured volume fraction was estimated using the law of propagation of uncertainty after determining the volume fraction of each species:

$$u_{\bar{X}_i} = \sqrt{\left(\frac{\partial \bar{X}_i}{\partial n_i} u_{n_i}\right)^2 + \left(\frac{\partial \bar{X}_i}{\partial n_{tot}} u_{n_{tot}}\right)^2} \quad (\text{A.1})$$

A coverage factor of 2 was applied to the combined uncertainty to produce a 95 % confidence interval.

### A.1 Number of Moles of a Given Species

The number of moles of a given species was determined from a calibration function of the integrated peak area of the respective species obtained from the TCD chromatogram. The Type A evaluation of standard uncertainty of the number of moles of a given species was taken as the standard deviation of the measurements obtained from the repeated tests. The Type B evaluation of standard uncertainty was determined from the error in the calibration functions for each species measured by the TCD further detailed in Appedix B. The combined uncertainty was found via quadrature:

$$u_{n_i} = \sqrt{u_{n_i, \text{cal}}^2 + s_{n_i}^2} \quad (\text{A.2})$$

### A.2 Total Number of Moles Identified

The total number of moles detected was determined from the summation of the number of moles for each species identified by the TCD. Therefore, the uncertainty in the total number of moles identified was the combined uncertainty of all the identified species via quadrature:

$$u_{n_{tot}} = \sqrt{\sum_{n=1}^N s_{n_i}^2} \quad (\text{A.3})$$

where  $N$  is the number of a species identified species in the TCD chromatogram.

## B. Uncertainty Analysis of Gas Species Calibrations

A calibration function is a relationship between an integrated peak area on the TCD chromatogram,  $Area_i$ , and the number of moles of a given species injected into the GC/MSD,  $n_i$ . A calibration function was determined by injecting a known amount of moles of a given species into the GC/MSD,  $n_{i,cal}$ , and identifying the peak area corresponding to the individual species. For this work, the calibration functions are approximately linear consisting of a slope,  $a$ , and intercept,  $b$ .

$$n_{i,cal} = a(Area_i) + b \quad (\text{B.1})$$

Calibration functions were weighted to account for the error of each gas standard used in the calibration procedure. The uncertainty of a calibration function was determined using the law of propagation of uncertainty:

$$u_{n_i} = \sqrt{\left(\frac{\partial n_i}{\partial a} u_a\right)^2 + \left(\frac{\partial n_i}{\partial b} u_b\right)^2} \quad (\text{B.2})$$

The uncertainties of the slope and intercept in a weighting linear regression are as follows:

$$u_a = \sqrt{\frac{\sum \frac{1}{u_{n_{i,cal}}^2}}{\left(\sum \frac{Area_i^2}{u_{n_{i,cal}}^2}\right)\left(\sum \frac{1}{u_{n_{i,cal}}^2}\right) - \left(\sum \frac{Area_i}{u_{n_{i,cal}}^2}\right)^2}} \quad (\text{B.3})$$

$$u_b = \sqrt{\frac{\sum \frac{Area_i^2}{u_{n_{i,cal}}^2}}{\left(\sum \frac{Area_i^2}{u_{n_{i,cal}}^2}\right)\left(\sum \frac{1}{u_{n_{i,cal}}^2}\right) - \left(\sum \frac{Area_i}{u_{n_{i,cal}}^2}\right)^2}} \quad (\text{B.4})$$

where  $u_{n_{i,cal}}$  is the uncertainty of the known number of moles of the respective species.

During calibration, the number of moles of a given species  $n_{i,cal}$  was calculated from the product of the total moles injected into the GC/MSD,  $n_{tot,inj}$  and the known concentration of the particular species in the calibration standard,  $C_i$ .

$$n_{i,cal} = C_i(n_{tot,inj}) \quad (\text{B.5})$$

A collection of gas calibration standards for a variety of species were pre-selected to provide a broad range of concentrations. All calibration standards were mixtures of the target gas species with a Nitrogen balance, with the exception of one standard balanced in Air. A list of gas standards used in this work, with their respective concentrations and Type B evaluation of standard uncertainty, is provided in Appendix B.2.

The uncertainty of the number of moles of a given species injected into the GC/MSD for calibration was estimated using the law of propagation of uncertainty:

$$u_{n_{i,cal}} = \sqrt{\left(\frac{\partial n_{i,cal}}{\partial C_i} u_{C_i}\right)^2 + \left(\frac{\partial n_{i,cal}}{\partial n_{tot,inj}} u_{n_{tot,inj}}\right)^2} \quad (\text{B.6})$$

### B.1 Total Moles Injected into the GC/MSD for Calibration

The total moles injected into the GC/MSD for calibration was determined from the pressure,  $P$ , temperature,  $T$ , and volume,  $V$ , of the gas sample injected into the GC/MSD using the experimental setup described in Section 2.2. The injected sample was assumed to be an ideal gas:

$$n_{tot,inj} = \frac{PV}{RT} \quad (\text{B.7})$$

where  $R$  is the universal gas constant (287 J/(mol · K)).

Pressure and temperature measurements were made using an Omega Digital Pressure Gauge (DPG409-030DWU) and K Type Thermocouple located at the GC/MSD Sample Loop injection valve, respectively, sampling at 2 Hz for 50 s. The volume of the GC/MSD sample loop,  $V_{sl}$ , was assumed to be 2 ml. The Type A evaluation of uncertainty of the total moles injected into the GC/MSD for calibration was determined from the standard error of the pressure,  $s_P$ , and temperature,  $s_T$  readings from the sampling period. The Type B evaluation of uncertainty for the total moles injected into the GC/MSD for calibration is determined from the bias error sources in the instrumentation,  $u_{inst}$ , used to measure pressure (0.008% accuracy of the reading), temperature (1.5 °C), and volume (0.02 ml) of gas sample injected. The combined uncertainty of the pressure, temperature, and volume was found via quadrature:

$$u_P = \sqrt{u_{inst}^2 + s_P^2} \quad (\text{B.8})$$

$$u_T = \sqrt{u_{inst}^2 + s_T^2} \quad (\text{B.9})$$

$$u_{V_{sl}} = \sqrt{u_{inst}^2} \quad (\text{B.10})$$

The standard uncertainty of the total moles injected into the GC/MSD for calibration was estimated using the law of propagation of uncertainty:

$$u_{n_{tot,inj}} = \sqrt{\left(\frac{\partial n_{tot,inj}}{\partial P} u_P\right)^2 + \left(\frac{\partial n_{tot,inj}}{\partial T} u_T\right)^2 + \left(\frac{\partial n_{tot,inj}}{\partial V_{sl}} u_{V_{sl}}\right)^2} \quad (\text{B.11})$$

## B.2 Table of Gas Standards with Error

A table of the gas standards with their respective concentrations and Type B evaluation of standard uncertainty, used for calibrating the GC/MSD is provided below. Lot numbers for all standards are provided for traceability.

**Table 2.** Gas Standards used to Calibrate GC/MSD

Components	Uncertainty(%)	Distributor	Lot No.
200 ppm Acetone	2.00	Gasco Affiliates, LLC.	DNJ-ACE-200N-1
0.26% Acetylene	2.00	Gasco Affiliates, LLC.	FBJ-M24-0.25%-1
1.04% Acetylene	2.00	Gasco Affiliates, LLC.	FBJ-M24-1
1.02% Argon	2.00	Gasco Affiliates, LLC.	DBJ-2-1N-1
88.5% Argon	2.00	Gasco Affiliates, LLC.	DBJ-2-90N-1
100 ppm Benzene	2.00	Gasco Affiliates, LLC.	FBJ-21-100-3
15.6% Carbon Dioxide	0.04	NIST Gas Sensing Metrology Group	9-C-44
24.5% Carbon Dioxide	2.00	Gasco Affiliates, LLC.	KBI-35-25-1
1.00% Carbon Dioxide	2.00	Matheson Tri-Gas	9306620888
2.51% Carbon Dioxide	2.00	Roberts Oxygen	1002080917
7.00% Carbon Dioxide	2.00	Roberts Oxygen	1009010318
0.30% Carbon Monoxide	2.00	Roberts Oxygen	1009010318
9.00% Carbon Dioxide	2.00	Praxair Distribution Inc.	304113044702
0.02% Carbon Monoxide	2.00	Matheson Tri-Gas	9306620888
0.11% Carbon Monoxide	2.00	Roberts Oxygen	1002080917
4.00% Carbon Monoxide	2.00	Praxair Distribution Inc.	304113044702
7.81% Carbon Monoxide	0.02	NIST Gas Sensing Metrology Group	51-28-C
0.51% Ethane	2.00	Gasco Affiliates, LLC.	FBJ-62N-0.5-1
1.00% Ethane	2.00	Gasco Affiliates, LLC.	FBJ-152N-1-1%-1
2.55% Ethane	2.00	Gasco Affiliates, LLC.	FBJ-152N-2.5-1
0.51% Ethylene	2.00	Gasco Affiliates, LLC.	FBJ-62N-0.5%-1
1.02% Ethylene	2.00	Gasco Affiliates, LLC.	FBJ-62N-1%-1
2.55% Ethylene	2.00	Gasco Affiliates, LLC.	FBJ-62N-2.5%-1
0.26% Hydrogen	2.00	Gasco Affiliates, LLC.	FBJ-84-0.25-1
0.50% Hydrogen	2.00	Gasco Affiliates, LLC.	KBI-84-0.5-1
1.00% Hydrogen	2.00	Gasco Affiliates, LLC.	KBI-84-1-3
2.00% Hydrogen	2.00	Gasco Affiliates, LLC.	FBJ-84-2-5
4.03% Hydrogen	2.00	Gasco Affiliates, LLC.	FBJ-84-4-2
0.40% Methane	2.00	Gasco Affiliates, LLC.	DBJ-135N-0.4-1
3.95% Methane	2.00	Gasco Affiliates, LLC.	DBJ-135N-4-2
40.8% Methane	2.00	Gasco Affiliates, LLC.	DBJ-135N-40-1
0.50% Oxygen	2.00	Gasco Affiliates, LLC.	DBJ-2-90N-1
1.97% Oxygen	0.01	NIST Gas Sensing Metrology Group	73-D-03
5.02% Oxygen	2.00	Gasco Affiliates, LLC.	DBJ-161-5-5
9.92% Oxygen	0.02	NIST Gas Sensing Metrology Group	72-D-60
10.2% Oxygen	2.00	Gasco Affiliates, LLC.	KBI-161-10-6
20.7% Oxygen	0.04	NIST Gas Sensing Metrology Group	71-D-51
0.42% Propane	2.00	Gasco Affiliates, LLC.	DBJ-176N-0.4-1
39.6% Propane	2.00	Gasco Affiliates, LLC.	DBJ-176N-40-1

### B.3 Concentration of Vapors from Bubblers

Liquid material concentrations were calibrated from the ratio of the liquid-vapor pressure to the total pressure injected into the GC/MSD.

$$C_{vap} = \frac{P_{vap}}{P} \quad (\text{B.12})$$

The vapor pressure of any given liquid can be calculated and modified using the bubbler setup shown in Fig. 10:

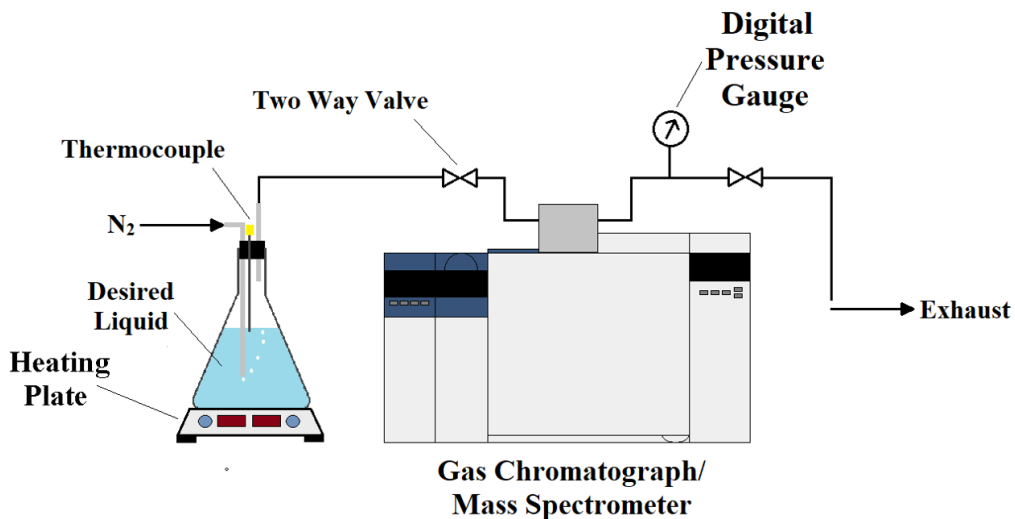


**Fig. 10.** Flow diagram for bubble calibration system used for liquid materials (acetone, ethanol, methanol, and water)

Nitrogen, acting as a carrier gas, was bubbled at the bottom of a liquid bath which after reaching the liquid surface transport vapor molecules through a heated gas line and into the GC/MSD sample loop. The concentration of the vapor injected into the GC/MSD was calculated from a liquid-vapor pressure correlation provided by DIPPR®.

$$P_{vap} = e^{A + \frac{B}{T} + C \ln T + D T^E} \quad (\text{B.13})$$

In this correlation,  $P_{vap}$  is the vapor pressure calculated from the temperature of the liquid bath,  $T$ , with the coefficients ( $A, B, C, D, E$ ) specific to the liquid material. Table 3 lists all coefficients for each calibrated liquid, including the uncertainty of their respective correlations,  $u_{corr}$ .

The concentration range of each calibrated liquid typically spanned between 2 % and 50 %. Liquid bath temperatures were controlled using a heating plate positioned underneath

**Table 3.** Liquid Vapor Pressure Correlation Coefficients for Various Calibrated Liquids

Liquid Material	A	B	C	D	E	Uncertainty(%)
Acetone	69.006	-5599.6	-7.0985	6.2237E-6	2.00	3.00
Ethanol	73.304	-7122.3	-7.1424	2.8853E-6	2.00	1.00
Methanol	82.718	-6904.5	-8.8622	7.4664E-6	2.00	3.00
Water	73.649	-7258.2	-7.3037	4.1653E-6	2.00	0.20

the insulated bubbler. The temperature of the bath,  $T_b$ , was measured using a K Type thermocouple placed at the liquid bath's surface. The liquid bath temperature measurements were sampled at 2 Hz for 50 s simultaneously with pressure and temperature measurements of the GC/MSD sample loop. Liquid-vapor calibrations were conducted once the bath a steady-state temperature (approximately 1 hour) and the Nitrogen/vapor gas mixture has swept through the GC/MSD sample loop. Upon injection into the GC/MSD, pressure and temperature measurements of the sample loop are made as previously describe in Appendix B.1.

The uncertainty of the concentration determined using Eq. B.12 was estimated using the law of propagation of uncertainty:

$$u_{C_{vap}} = \sqrt{\left(\frac{\partial C_{vap}}{\partial P} u_P\right)^2 + \left(\frac{\partial C_{vap}}{\partial P_{vap}} u_{P_{vap}}\right)^2} \quad (\text{B.14})$$

The uncertainty of the pressure measured upon injected was calculated from Eq. B.8. The uncertainty of the vapor pressure was found by combining the propagated error of liquid bath temperautre and the uncertainty in the correlation via quadrature:

$$u_{P_{vap}} = \sqrt{\left(\frac{\partial P_{vap}}{\partial T_B} u_{T_B}\right)^2 + u_{corr}^2} \quad (\text{B.15})$$

The Type A evaluation of uncertainty of the liquid bath temperautre readings is determined from the standard error of the temperature,  $s_{T_B}$  readings from the sampling period. The Type B evaluation of uncertainty for the liquid bath temperature was the bias error source ( $1.5^\circ\text{C}$ ) in the thermocouple,  $u_{inst}$ . The combined uncertainty liquid bath temperature was determined via quadrature:

$$u_{T_B} = \sqrt{u_{inst}^2 + s_{T_B}^2} \quad (\text{B.16})$$

### C. Uncertainty Analysis of the Soot Mass Fraction

The local soot mass fraction measurements,  $M_s$  made at various heights above the fuel surface in pool fires of different fuels were calculated through a combination of Eq. 5, 6, and 7:

$$M_s = \frac{m_s V_{sl}}{\dot{V} t m_{tot}} \frac{T_\infty}{T_p} \quad (\text{C.1})$$

where  $m_s$  is the mass of soot collected on the PTFE filter and gun cleaning patches,  $\dot{V}$  is the volumetric flow rate measured by the mass flow controller,  $V_{sl}$  is the volume of the sample loop,  $\sum n_i \cdot MW_i$  is the total mass of the gas sample detected in the TCD chromatogram calculated from the summation of the product of the number of moles of a given species and their respective molar mass,  $T_\infty/T_p$  is the ratio of the internal gas flow temperature readings of the mass flow controller to the temperature of the probe, and  $t$  is the total sampling time. The uncertainty of the measured soot mass fraction was estimated using the law of propagation of uncertainty after determining the soot mass fraction:

$$u_{M_s} = \sqrt{\left(\frac{\partial M_s}{\partial m_s} u_{m_s}\right)^2 + \left(\frac{\partial M_s}{\partial \dot{V}} u_{\dot{V}}\right)^2 + \left(\frac{\partial M_s}{\partial V_{sl}} u_{V_{sl}}\right)^2 + \left(\frac{\partial M_s}{\partial m_{tot}} u_{m_{tot}}\right)^2 + \left(\frac{\partial M_s}{\partial T_\infty} u_{T_\infty}\right)^2 + \left(\frac{\partial M_s}{\partial T_p} u_{T_p}\right)^2} \quad (\text{C.2})$$

A coverage factor of 2 was applied to the combined uncertainty to produce a 95 % confidence interval.

#### C.1 Mass of Soot

The mass of soot was measured from the difference in mass of a dried PTFE filter and dried gun cleaning patches immediately before and 48 hrs after each test. The Type A evaluation of standard uncertainty of the mass of soot,  $m_s$  was taken as the standard deviation,  $s_{m_s}$ , of the measurements sampled three times before and after each test. The Type B evaluation of Uncertainty was determined from the instrumentation error sources of the scale and was found to be  $u_{inst} = 1\%$  of the reading. The combined uncertainty was found via quadrature:

$$u_{m_s} = \sqrt{u_{inst}^2 + s_{m_s}^2} \quad (\text{C.3})$$

#### C.2 Mass Flow Controller Volumetric Flow Rate

A mass flow controller was used to measure the volumetric flow rate,  $\dot{V}$ , within the gas sampling line. The Type A evaluation of standard uncertainty was taken as the standard deviation of the flow measurements sampled at 2 Hz during the gas sampling period which varied from 12 min to 25 min depending on the sampling location within the fire. The Type B evaluation of standard uncertainty was determined from the calibration error,  $u_{cal}$ , and the precision error sources at calibration conditions,  $u_p$ , defined as 2 ml and 0.8 % of

the reading + 0.2 % of the full scale (2 Lpm), respectively. The combined uncertainty is calculated via quadrature:

$$u_V = \sqrt{u_p^2 + u_{\text{cal}}^2 + s_V^2} \quad (\text{C.4})$$

### C.3 GC/MSD Sample Loop Volume

All gas sampling experiments and calibrations were conducted using a 2 ml sampling loop. The Type B evaluation of standard uncertainty of the GC/MSD sample loop volume was assumed to be 1 %.<sup>1</sup>

### C.4 Total Mass Injected into the GC/MSD

The total mass detected in the TCD chromatogram,  $m_{tot}$ , was calculated from the summation of products of the moles of given species and their respective molar mass,  $MW_i$ :

$$m_{tot} = \sum_{n=1}^N n_i \cdot MW_i \quad (\text{C.5})$$

The uncertainty in the total mass detected was defined as the combined uncertainty of all identified species multiplied by their corresponding molar mass via quadrature:

$$u_{m_{tot}} = \sqrt{\sum_{n=1}^N (s_{n_i} \cdot MW_i)^2} \quad (\text{C.6})$$

where  $N$  is the number of a species identified species in the TCD chromatogram.

### C.5 Mass Flow Controller Internal Gas Flow Temperature Reading

The mass flow controller provides an internal gas flow temperature reading that was recorded manually during the gas sampling process. The uncertainty of the temperature reading was determined from the Type B evaluation of standard uncertainty of the mass flow controller temperature measurement defined as 0.75 % of the reading.

### C.6 Temperature Reading at the Entrance of the Probe

---

<sup>1</sup>The uncertainty of the sample loop was assumed to be 1 % after contacting the manufacturer.

#### D. Uncertainty Analysis of the Mixture Fraction

The mixture fraction,  $Z$ , was determined from Eq. 8 based on carbon containing species. The uncertainty of the determined mixture fraction was estimated using the law of propagation of uncertainty based on calculated mass fractions,  $Y_i$ .

$$u_Z = \sqrt{\sum_{i=1}^N \left( \frac{\partial Z}{\partial Y_i} u_{Y_i} \right)^2} \quad (\text{D.1})$$

## E. Uncertainty Analysis of Pool Fire Parameters

### E.1 Mass Burning Flux

The mass burning flux,  $m''$ , was measured from the mass loss rate of the fuel reservoir, feeding to the pool burner via gravity, during the burning period per area of the pool burner. The area of the pool burner,  $A$ , was assumed to be 30 cm. Mass measurements were made using a Precisa XB-6200C Precision XB Laboratory Prime Balance sampling at 1 Hz for the entire duration of the burning period. The balance was calibrated from a collection standard weights. The expanded uncertainty was estimated via quadrature from a combination of the Type A and Type B evaluation of standard uncertainty. The Type A evaluation of standard uncertainty was calculated from the standard error,  $s_{m_f}$  of the time-averaged mass loss measured during the burning period. The Type B evaluation of standard uncertainty was determined from the bias error of the balance,  $u_{\text{inst}}$  (0.01 g), and the calibration error,  $u_{\text{cal}}$  (1 % of the reading).

$$u_{m''} = \frac{1}{A} \sqrt{s_{m_f}^2 + u_{\text{inst}}^2 + u_{\text{cal}}^2} \quad (\text{E.1})$$

### E.2 Heat Release Rate

The heat release rate was determined from Eq. 1 using the heat of combustion property of the respective fuel, provided by DIPPR®, and time-averaged mass burning flux values listed in Table 1. The uncertainty of the heat release rate was calculated via the law of propagation of uncertainty:

$$u_{\dot{Q}} = \sqrt{\left( \frac{\partial \dot{Q}}{\partial m''} u_{m''} \right)^2 + \left( \frac{\partial \dot{Q}}{\partial \Delta H_c} u_{\Delta H_c} \right)^2} \quad (\text{E.2})$$

### E.3 Mean Flame Height

The mean flame height,  $u_{h_f}$ , was determined by measuring the distance between the pool surface and flame tip using the photographic analysis method described in Section ???. The uncertainty of the mean flame height,  $u_{h_f}$ , was calculated from a combined uncertainty of the Type A and B evaluation of standard uncertainty. The Type A evaluation of standard uncertainty was estimated from the standard deviation of the height measurements,  $s_{h_f}$ , made with each frame. The error of the measured distance using the photographic analysis method compared to the true distance,  $u_{\text{meth}}$ , was found to be 0.1% and was treated as the Type B evaluation of standard uncertainty. The combined uncertainty calculation of the mean flame height is shown below:

$$u_{h_f} = \sqrt{s_{h_f}^2 + u_{\text{meth}}^2} \quad (\text{E.3})$$